Rare but not absent: the Inverted Mitogenomes of Deep-Sea Hatchetfish

André Gomes-dos-Santos[1], Nair Vilas-Arrondo[2,3], André M. Machado[1], Esther Román-Marcote[3], Jose Luís Del Río Iglesias[3], Francisco Baldó[4], Montse Pérez[3], Miguel M. Fonseca[1], L. Filipe C. Castro[1,5*] and Elsa Froufe[1*]

[1]CIIMAR/CIMAR - Interdisciplinary Centre of Marine and Environmental Research, University of Porto, Matosinhos, Portugal

[2] Programa de Doctorado "Ciencias marinas, Tecnología y Gestión" (Do*MAR), Montse Pérez Facultad de biología, Universidad de Vigo, Vigo, Spain

[3] Centro Oceanográfico de Vigo Instituto Español de Oceanografía (IEO, CSIC). Subida a Radio Faro, 50. 36390 Vigo (Pontevedra), Spain

[4] Centro Oceanográfico de Cádiz, Instituto Español de Oceanografía (IEO, CSIC), Puerto pesquero, dársena de Levante s/n, 11006 Cádiz, Spain

[5] Department of Biology, Faculty of Sciences, University of Porto, Porto, Portugal

* Corresponding authors: Elsa Froufe elsafroufe@gmail.com and L. Filipe C. Castro lfilipecastro@gmail.com

Abstract

Mitochondrial genomes are by definition compact and structurally stable over aeons. This generalized perception results from a vertebrate-centric vision, as very few types of mtDNA rearrangements have been described in vertebrates. By combining a panel of sequencing approaches, including short- and long-reads, we show that species from a group of illusive marine teleosts, the deep-sea hatchetfish (Stomiiforms: Sternoptychidae), display a myriad of new mtDNA structural arrangements. We show a never reported inversion of the coding direction of protein-coding genes (PGG) coupled with a strand asymmetry nucleotide composition reversal directly related to the strand location of the Control Region (which includes the heavy strand replication origin). An analysis of the 4-fold redundant sites of the PCGs, in thousands of vertebrate mtDNAs, revealed the rarity of this phenomenon, only found in 9 fish species, five of which are deep-sea hatchetfish. Curiously, in Antarctic notothenioid fishes (Trematominae), where a single PCG inversion (the only other record in fish) is coupled with the inversion of the Control Region, the standard asymmetry is disrupted for the remaining PCG but not yet reversed, suggesting a transitory state in this species mtDNA. Together, our findings hint that a relaxation of the classic vertebrate mitochondrial structural *stasis*, observed in Sternoptychidae and Trematominae, promotes disruption of the natural balance of asymmetry of the mtDNA. Our findings support the long-lasting hypothesis that replication is the main molecular mechanism promoting the strand-specific compositional bias of this unique and indispensable molecule.

45 **Keywords:** mitogenome; strand asymmetry; deep-sea fish; vertebrate; mitochondrial

46 gene order; rearrangements.

47

Introduction

Counterintuitively, the mitochondrial genome (mtDNA) is far more variable than normally recognized, including structure, gene content, order and orientation, organization and mode of expression (Shtolz and Mishmar 2023). In Metazoa, several types of mtDNA are described, including linear telomeric molecules (e.g., Cnidaria), “giant” circular molecules (e.g. some Bivalvia and Placozoa) and several mini-circular molecules (e.g. Insecta) (Kolesnikov and Gerasimov 2012; Shtolz and Mishmar 2023). In vertebrates, the classic mtDNA is described as a compact circular molecule, maternally inherited, between 16–19 kbp and two compositionally distinct strands, conventionally referred to as heavy (H-strand with high G composition) and light (L-strand with low G composition) (Clayton 1982; Boore 1999; Kolesnikov and Gerasimov 2012). The standard vertebrate mtDNA encodes 37 genes, 13 protein-coding genes (PCG); two ribosomal RNAs (rRNAs); 22 transfer RNAs (tRNAs); and two differently located and strand-specific replication origins (heavy strand replication origin [OH] and light strand replication origin [OL]) (Clayton 1982; Lee et al. 1995; Boore 1999; Kolesnikov and Gerasimov 2012). The OH is placed within a larger non-coding region, the Control Region (CR), which includes several regulators of the mtDNA replication and transcription and where four evolutionary conserved sequence blocks are commonly found (i.e, CSB-I, CSB-II, CSB-III, and CSB-D) (Clayton 1982; Lee et al. 1995; Boore 1999; Kolesnikov and Gerasimov 2012). The 13 mtDNA PCG, which follows the standard architecture (i.e., number, relative positioning and coding strand), play key functional roles in the oxidative phosphorylation (OXPHOS) cascade (Clayton 1982; Boore 1999; Kolesnikov and Gerasimov 2012).

Exceptions to this generalized picture, in vertebrate classes, are extremely rare, with very few and small-scale deviations (Gissi et al. 2010; Zhang et al. 2020; Formenti et al. 2021; Montaña-Lozano et al. 2022; Sharbrough et al. 2023; Shtolz and Mishmar 2023). Among the different groups, birds and reptiles show the highest distribution of rearranged genes, while mammals and fish show residual examples of rearrangements (Zhang et al. 2020; Montaña-Lozano et al. 2022; Shtolz and Mishmar 2023). In fish, three distinct types of mtDNA gene rearrangements have been described recently by Satoh et al. (2016): “shuffling”, i.e., local position change maintaining coding polarity (i.e., genes coding strand); “translocation”, i.e., movement to a distinct location maintaining the genes encoded strand; and the rarest event “inversions”, i.e., genes (or non-coding unities) switch to their complementary strand (Fonseca et al. 2008; Kong et al. 2009; Gong et al. 2013; Fonseca et al. 2014; Arrondo et al. 2020; Papetti et al. 2021; Shtolz and Mishmar 2023). Inversions, when acting upon the replication controlling unities (i.e., the CR or OH), have been shown to promote a switch of the strand asymmetry nucleotide composition. Consequently, The mtDNA replication is suggested to be involved in the differently accumulated strand mutation patterns of the mtDNA (assuming an asymmetric model of mtDNA replication) (Fonseca et al. 2008; Fonseca et al. 2014; Shtolz and Mishmar 2023). Marine deep-sea hatchetfish from the family Sternoptychidae (Order: Stomiiformes) are a group of small (less than 100 mm) and peculiar mesopelagic fishes (Nelson 2016). The family consists of two subfamilies, Maurolicinae and Sternoptychinae, which include around 70 species distributed through 10 genera (Howell and Krueger 1987; Nelson 2016; Coad 2019). These species are generally found in high abundance and biomass within the mesopelagic ichthyofauna and with important ecological functions and a key trophic position (Gjoesaeter and Kawaguchi 1980;

Eduardo et al. 2020). Species from the family Sternoptychidae have been described as "*some of the most bizarre stomiiforms*" and are characterized by having a condensed body with a reflecting fattened silver side that allows camouflage (Carnevale 2008). As in all other Stomiiformes, deep-sea hatchetfish possess specialized bioluminescent organs, i.e., photophores that allow them to produce light (Krönström et al. 2005; Carnevale 2008; Haddock et al. 2009).

Here we describe four new Sternoptychidae whole mtDNA, using Illumina PE short reads and Oxford Nanopore long reads, showing that the mtDNA of Sternoptychidae have a diverse and unusual gene architecture. Our findings include mtDNA gene shuffling, translocation and inversions, acting on PCG, tRNA rRNA and/or CR. In particular, we demonstrate that strand asymmetry nucleotide composition reversal occurs when genes change their coding polarity relative to the Control Region (i.e. OH, initiation of replication). Conversely, inversions of CR were shown to promote the complete nucleotide strand asymmetry reversal in two deep-sea hatchetfish species. Moreover, by investigating over 6000 species we determine that strand asymmetry is a rare event in vertebrate mitochondrial genomes. In Antarctic notothenioid fishes (Trematominae), a PCG inversion (the only case previously reported in fish) coupled with the CR inversion is shown to disrupt the standard asymmetry for the remaining PCG. Together, our findings provide strong evidence supporting the long-lasting theory that replication is the main molecular mechanism promoting the strand-specific compositional bias of the mtDNA.

Results and Discussion

Deep-sea hatchetfish mtDNA show a widespread complex repetitive region hampering full sequence circularization

We generated four novel whole mitochondrial genomes from the marine hatchetfish, two of them resulting from new nuclear genome assemblies: *Argyropelecus aculeatus* Valenciennes, 1850 (lovely hatchetfish), *Argyropelecus hemigymnus* Cocco, 1829 (half-naked hatchetfish), *Argyropelecus olfersii* (Cuvier, 1829) and *Maurolicus muelleri* (Gmelin, 1789) (Mueller's pearlside). The raw sequencing reads and mtDNA assemblies were deposited at NCBI, and respective SRA and assembly accessions are depicted in Table 1 and linked to BioProject PRJNA977192 (Provisory Reviewer Link https://dataview.ncbi.nlm.nih.gov/object/PRJNA977192?reviewer=qp1erbs33ac430jhnvu9demc1m).

The mtDNA lengths varied from 15,230 bp in *M. muelleri* to 23,291 bp in *A. aculeatus*, largely influenced by poorly resolved repetitive regions, which includes the putative CR and long species-specific intergenic regions (figs 1-3). The only previously assembled hatchet fish mtDNA with a CR annotation is *Polyipnus polli* Schultz, 1961 (AP012962.1) (fig. 1). Conversely, in other publicly available mtDNAs, the CR was either not annotated, i.e., in *Sternoptyx obscura* Garman, 1899 (OP057081.1) and in *Sternoptyx diaphana* Hermann, 1781 (MT588184.1) (fig. 2), or not sequenced, i.e., in *M. muelleri* (AP012963.1) and *Argyropelecus affinis* Garman, 1899 (AP012964.1) (fig 1). The difficulty in obtaining this region has already been observed in many other animal groups (e.g., (Ghiselli et al. 2021)). Conversely, in the three novel *Argyropelecus sp.* sequenced mtDNAs, i.e., *A. aculeatus*, *A. hemigymnus*, and *A. olfersii*, long intergenic repeats were identified (fig. 3). The

difficulty in resolving these repetitive regions using short reads prevented the assembly of a single contig in *A. olfersii* (composed of two contigs), as well as the circularization of the *A. hemigymnus* assembly (fig. 3). This factor also hampered the assembly of the recently published *S. diaphana* mtDNA, which required scaffolding with Sanger sequencing (Arrondo et al. 2020). Nevertheless, we efficiently identified the CSB-II (thus the CR) in all but one (i.e., *A. olfersii*) (Supplementary File 1 and fig. S1).

Sequencing approaches are key for resolving complex mtDNA assemblies (e.g. (Calcino et al. 2020; Formenti et al. 2021)). Consequently, in *A. aculeatus* we used Oxford Nanopore long-reads to determine the composition of the complete mtDNA molecule. The produced reads were highly efficient in resolving the full mtDNA sequence, with some reads even spawning the entire molecule, supporting the inferred architecture. The final assembly was circularized, revealing two long repetitive regions, one spawning ~4800 bp, which included the CSB-II (between tRNA-Asp and tRNA-Pro) and the other ~1750 bp (between tRNA-Phe and a COI) (figs 3 and S2). As for the other two *Argyropelecus sp.*, although the short-read assemblies retrieved all the mtDNA genes, the aforementioned repetitive regions were fragmented (fig. 3).

Gene shuffling, translocations, duplications and inversions define the structure of mtDNA structure in deep-sea hatchetfish

We next investigated the gene content and overall structure of the mtDNA in deep-sea hatchetfish. The newly sequenced genomes as well as those deposited in GenBank show striking deviations from the standard vertebrate gene arrangement

(figs 1-3). While the mtDNA from three species, i.e., *M. muelleri, A. affinis* and *P. polli*, maintain the standard vertebrate mtDNA architecture (fig. 2), most of the newly sequenced mtDNA revealed considerably modified architectures (figs 2-3) (Saccone et al. 2002; Satoh et al. 2016). The results show that shuffling, translocation and inversion of PCGs, rRNAs and more abundantly tRNAs, are widespread in the mtDNA deep-sea hatchetfish (figs 2-3). Even within the same genus, high structural differences can be detected (figs 2-3). Species from the *Argyropelecus* genus show four distinct mtDNA architectures: one maintains the standard vertebrate structure; while the other three share a radical inversion of a large fragment composed of several genes, with reciprocal additional unique features (fig. 3). This fragment includes the inversion of the PCGs ND2 and ND1, the rRNA 16S and 12S and several tRNAs (M, I, L1, V and F), as well as the shuffling of two tRNAs (A and C) (fig. 3). The inversion of two PCGs has never been reported in fish mtDNA before. To date, the only reported inversion of a PCG is of ND1 in a single clade of Antarctic notothenioid fishes (Nototheniidae: Trematominae) (Papetti et al. 2021; Minhas et al. 2023). Interestingly, this also resulted from the inversion of a large fragment, which included the rRNA genes, several tRNAs (E, I, L2, V and F) as well as the CR (Papetti et al. 2021; Minhas et al. 2023).

Some species-specific tRNA duplications were observed (figs. 2-3). The most striking of these duplications was captured by the Nanopore-based assembly in *A. aculeatus*, corresponding to a tandem duplication of two tRNAs C-A, followed by one tRNA C. This pattern seems to also occur in *A. olfersii*, in which a shorter tandem duplication of two tRNAs C-A was present, while in *A. hemigymnus* the two tRNAs are present in the same location but in a single copy (fig. 3). Furthermore, *A. hemigymnus* shows a unique shuffling of the ND6 and the tRNA E (fig. 2). The two *Sternoptyx sp.* revealed

196 the overall same mtDNA architecture, with *S. obscura* having duplications and
197 "*pseudogenization*" of ND3 and 16S (fig. 2). Gene duplication in mtDNA is often
198 followed by the loss of one the copies, frequently retaining fragments of the original
199 duplicated gene (Satoh et al. 2016; Papetti et al. 2021).
200
201 **Phylogenetic Analysis shows poorly resolved deep-sea hatchetfish**
202 **evolutionary relationships**
203
204 We next analysed the phylogenetic relationships between the various deep-sea
205 hatchetfish species. The resulting phylogenetic inference, rooted with *Coregonus*
206 *lavaretus* (Linnaeus, 1758) (following (Ijichi et al. 2018; Arrondo et al. 2020)), is split
207 into two major groups, one composed of order Stomiiformes and the other composed
208 of families Synodontidae, Ateleopodidae, Myctophidae and Trachipteridae (fig. 4).
209 Stomiiformes' phylogenetic relationships are poorly revolved, with very low support in
210 most of the nodes. Within deep-sea hatchet fish, i.e., family Sternoptychidae, the
211 relationships among the genus are also poorly resolved and an unexpected long
212 branch is seen for the two S*ternoptyx* species (fig. 4). The low support persisted in
213 the amino acid-based phylogeny (fig. S3). The mtDNA phylogeny here presented is
214 the first to include more than one species of the deep-sea hatchet fish (see (Arrondo
215 et al. 2020)). However, the taxon representation is still incomplete, which likely
216 explains the low support observed. The relationships of the four *Argyropelecus sp.*
217 are well resolved and reflect the structural mtDNA variation here described (figs. 1-3).
218 *Argyropelecus affinis*, the only species to preserve the standard vertebrate structure
219 is the first split within the genus, followed by *A. hemigymnus*, sister to *A. olfersii* + *A.*
220 *aculeatus*, the two most structurally similar (fig. 4).

To obtain a more taxa-representative phylogeny, all the cytochrome oxidase subunit I (COI) sequences available on GenBank were used (fig. 3). The COI alignment included a total of 261 sequences (total length of 652 bp) (Supplementary File 2), from 26 distinct deep-sea hatchetfish species and the outgroup species, i.e., *Coregonus clupeaformis* (Mitchill, 1818). The resulting nucleotide phylogeny shows once again low support among inter-genus relationships (fig. 4). Even though this phylogeny includes 260 sequences from marine hatchetfish, it highlights the need to increase the molecular data for the whole group.

GC/AT skew of strand-specific 4-fold redundant sites show a strikingly frequent strand asymmetry reversal in deep-sea hatchetfish always coupled with CR strand relative position

The mtDNA asymmetric strand nucleotide composition of the H and L strands is generally highly demarked in vertebrates, with a strong signature in the A-T and C-G composition of each stand (Saccone et al. 2002). This pronounced signature is the distinguishable factor between the two strands, i.e., the H(heavy)-strand, which is guanine rich, and L(light)-strand, which is guanine poor (Francino and Ochman 1997). Conversely, inverted genes, i.e., genes that change to the complementary strand, will be exposed to the mutational bias specific of the new strand, and thus are expected to change their mutational signature accordingly, as proposed by the asymmetric model of mtDNA replication (Fonseca et al. 2008; Kennedy et al. 2013; Fonseca et al. 2014).

Given the newly detected inversions of two PCGs in *A. aculeatus*, *A. hemigymnus*, and *A. olfersii*, as well as the oddly long branch lengths observed in *Sternoptyx sp.*,

we next estimated the GC/AT skew of the PCGs at the 4-fold redundant sites (the most likely to accumulate strand-specific mutations and to reflect the underlying mutational processes given that selection acting on these sites is weaker) for all the marine hatchetfish under study.

As expected, in the mtDNA that maintains the standard vertebrate architecture with no detectable structural changes, i.e., *M. muelleri*, *A. affinis* and *P. polli*, shows the AT/GC skew pattern of a gene encoded in the L-strand (fig. 5 and S4, i.e., AT skew < 0 and GC skew > 0). Interestingly, in the two *Argyropelecus sp.* with inverted PCG polarity, this AT/GC skew pattern was observed in ND6, but also in ND1 and ND2, the two PCGs included in the inverted fragment (fig. 5 and S4). Most strikingly, for the two *Sternoptyx sp.*, the entire AT/GC skew pattern is reversed in all PCGs (fig. 5 and S4) but with no rearrangements or inversions detected in those genes. What could be causing the AT/GC skew reversion in these genomes? To date, such phenomenon, in vertebrates, has been suggested to result from CR inversion, and from the replication mechanism itself with the leading strand becoming the lagging strand and vice-versa during an asymmetric mode of replication (Fonseca et al. 2008; Fonseca et al. 2014). We tested this hypothesis by characterising the relative positioning of the initiation of replication and by identifying elements that have been described to be key in the replication mechanism of vertebrate mtDNA: the conserved sequence blocks CSB-II and III. Typically, CSB-II consists of six or more cytosines, one thymine and one adenine ending with five or more cytosines: 5'-CCCCCCTACCCCC – 3'. We used this sequence as a reference, allowing for some variation in the length of the poly-C flanks. CSB-III is less conserved, generally identified by its positioning regarding CSB-II, and may be absent in fish CR (Satoh et al. 2016). The Motif Discovery analysis identified CSB-II in all the analysed

sequences, except in *P. polli* while CSB-III was less prevalent, as previously observed by Satoh et al., (2016) (Supplementary File 1 and fig. S1). The absence of both CSBs in *P. polli* needs further evaluation, as this mitogenome is a direct submission to NCBI without detailed information on how it was generated. Astonishingly, as previously predicted, the orientation of the CSB-II and therefore of the CR relative to the PCG was the common denominator determining the AT/GC skew nucleotide asymmetry pattern (Supplementary File 1 and figs 1-3 and S1). That is, in the two *Sternoptyx sp.* the CSB-II is the only element changing its coding polarity (inversion), having the same polarity as ND6 and contrary to all other PCGs, while in the remaining species, the relative position follows the standard vertebrate architecture (Supplementary File 1 and figs 1-3 and S1).

To date, the only reported PCG inversion in a vertebrate is in one clade of Antarctic notothenioid fishes (Nototheniidae: Trematominae), consisting of the inversion of a large genomic segment (~5kbp), which includes four tRNAs, two rRNAs, the PCG inversion (ND1) and the CR (Kennedy et al. 2013; Papetti et al. 2021). Once again, the relative position of the CR, here identified through CSB-II (Supplementary File 1 and fig. S1), is the determining factor shaping the nucleotide strand asymmetry, i.e., ND1 is the only PCG with the same polarity as the CR and thus it is also the only PCG maintaining its AT/GC skew pattern, while the remaining genes show a completely disrupted pattern. Interestingly, the fact that the latter-mentioned PCG shows a disruption but not a reversal AT/GC skew pattern, suggests that, in this group of organisms, the process of the mtDNA nucleotide composition strand asymmetry reversal is still in a transitory state (fig. S5). A complete disruption of the typical strand asymmetry signature was detected in all 15 Trematominae mtDNA

295 available, while the remaining notothenioid fishes maintained the standard pattern
296 (fig. S5).
297 To access similar putative hidden patterns in other vertebrates, we next performed a
298 vertebrate-wide assessment of the AT/GC skew at 4-fold redundant sites (Fonseca et
299 al. 2008; Fonseca et al. 2014) in a total of 6,297 mtDNA (Retrieved from RefSeq in
300 May 2022). The results demonstrate that the complete reversal of the nucleotide
301 strand asymmetry composition is observed solely in the *Sternoptyx sp.* and those
302 previously reported by Fonseca et al., (2008, 2014), totalizing seven species (figs. 6
303 and S4). Moreover, single gene asymmetry reversal is detectable for the ND1 and
304 ND2 genes of the three *Argyropelecus* species here described (figs. 6 and S4).
305 Given that there are still many un-sequenced marine hatchetfish whole mtDNA, we
306 hypothesised that calculating the AT/GC skew pattern at 4-fold redundant sites for
307 the most sequenced mitochondrial gene of the group, i.e., COI, would be an
308 informative strategy regarding the whole family. The results also show the reversed
309 pattern in all analysed *Sternoptyx* species (n=4), thus suggesting the reversal of the
310 nucleotide strand asymmetry is shared by all analysed *Sternoptyx* (figs. 6 and S4).
311 The remaining hatchetfish species maintain the standard vertebrate AT/GC skew
312 pattern, which is also in accordance with the results deduced from whole mtDNA
313 assembly and annotation.
314
315 **Genomic *Oddities*: inverted mtDNA and large nuclear genomes**
316
317 The combination of sequencing methodologies allowed the determination of *de novo*
318 four mtDNA from deep-sea hatchetfish species. Strikingly, the sequential analysis of
319 gene annotation, phylogenetics, and AT/GC skew sequence investigations support a

unique case of mtDNA structural plasticity (Shtolz and Mishmar 2023). We expanded the analysis to include thousands of available mtDNA. Our findings show that partial or full mtDNA inversions are evolutionary restricted in a minute of unrelated fish clades: *Argyropelecus sp*. *Sternoptyx sp*. The immediate causes of this phylogenetically restricted alteration of mtDNA structure are unknown and deserve further exploration. In fact, within Metazoa, vertebrates show the strongest signs of purifying selection for gene rearrangement (Shtolz and Mishmar 2023), with recent studies suggesting that gene blocks inversions (only recorded in invertebrates) promote sticking changes in the transcriptional pattern, thus requiring new regulatory elements (Blumberg et al. 2014; Blumberg et al. 2017; Barshad et al. 2018; Shtolz and Mishmar 2023). Consequently, our highly unexpected findings raise the interesting possibility of an adaptive scenario of the reported mtDNA oddities. Interestingly, using the high-coverage whole genome sequencing for *A. aculeatus* and *S. diaphana* we were able to appraise the genome size for both species (fig. S6). The results show an unexpectedly large genome size estimation, with both species being approximately 2.70 Gbp long (fig. S6). Most teleost species have an average of 1 Gbp long genome size, with the exceptions being usually attributed to whole genome duplication events (Parey et al. 2022). Together, our results suggest that like the mitogenomes, the whole genome of deep-sea hatchetfish is also unusual and deserves future explorations.

Methods

Samples collection and DNA extraction

In total, four specimens were captured for this study, three from the genus *Argyropelecus*, i.e., *Argyropelecus aculeatus* Valenciennes, 1850, *Argyropelecus hemigymnus* Cocco, 1829, and *Argyropelecus olfersii* (Cuvier, 1829), and one from genus *Maurolicus*, i.e., *Maurolicus muelleri* (Gmelin, 1789). The specimens were obtained during the scientific surveys: EU Groundfish Survey (Platuxa-2019) in North Atlantic (43,1544 N- 51,4429 W, 2019); from the EU Groundfish Survey (Platuxa-2019) in the Northwest Atlantic Ocean (43,3838 N- 49,0036 W, 2019); from the Survey PORCUPINE20 In Porcupine Bank (51.0677 N; -14.2862 W, 2020) and from EU Groundfish Survey FN3L19 in North Atlantic (-47,668 N; 47,497833 W), respectively. Morphological identification was performed onboard and whole specimens are stored in absolute ethanol and are stored at DNA and Tissue bank at CIIMAR – Interdisciplinary Center of Marine and Environmental Research. The specimen treatment has been approved by the CIIMAR ethical committee and by CIIMAR Managing Animal Welfare Body (ORBEA) according to the European Union Directive 2010/63/EU. Whole genomic DNA for each specimen was obtained from a small portion of the muscle tissue using the Qiagen MagAttract HMW DNA extraction kit, following the manufacturer's instructions. For all samples, total DNA was used for Illumina paired-end (PE) library preparation and sequencing at the Macrogen, Inc. (Seoul, Korea), using Illumina HiSeq X Ten platform, with 150 bp PE configuration. For *A. aculeatus* and *S. diaphana* high coverage whole genome (WGS) PE sequencing was performed, while the remaining samples were only sequenced at low coverage. Furthermore, low-coverage Nanopore (Oxford Nanopore) genome skimming was performed for *A. aculeatus*. Briefly, ~1 µg of genomic DNA was used for library preparation using the LSK109 kit and after sequenced on an FLO-MIN106 revD SpotON R9.4 Flow Cell for 48 h.

370

371 **Whole mitogenome assemblies and annotation**

372 Raw Illumina PE reads were quality-filter and adaptors were removed using
373 Trimmomatic (version 0.38) (Bolger et al. 2014), using the parameters LEADING:5
374 TRAILING:5 SLIDINGWINDOW:5:20 MINLEN:36. Read quality was inspected before
375 and after trimming using FastQC (version 0.11.8)
376 (http://www.bioinformatics.babraham.ac.uk/projects/fastqc/).
377 Whole mitogenome reconstruction for each species was obtained using several
378 distinct approaches. For each species, assemblies were performed with
379 GetOrganelle v1.7.1 (Jin et al. 2020), specifying a multi k-mer approach (i.e., from
380 20-125 with a 5-mer increment). GetOrganelle is an interactive baiting pipeline that
381 filters mtDNA reads and uses the SPAdes assembler (Bankevich et al. 2012) to
382 reconstruct the mitogenome with the filtered reads. The results of the assemblies
383 were individually validated using multiple approaches. For cases where multiple
384 assemblies were generated, i.e., *A. hemigymnus*, and *A. olfersii*, the gfa files were
385 inspected using Bandage v0.8.1 (Wick et al. 2015) which revealed several
386 ambiguous disjoints. Furthermore, annotation was generated for some of the putative
387 assemblies using the module “annotate” from MitoZ v.3.4 (Meng et al. 2019), which
388 showed that the ambiguous disjoints were localized within no-coding repetitive
389 regions. Consequently, new assemblies were performed, first using larger k-mer with
390 GetOrganelle v1.7.1 and if the problem persisted, using metaSPAdes v3.12.0 (Nurk
391 et al. 2017) with the maximum K-mer size possible, i.e., 127. In the end, the selected
392 best representative assemblies for each species were as follows, for *M. muelleri* the
393 GetOrganelle assembly with multi k-mer (20-125-mer with a 5-mer increment), for *A.*
394 *olfersii* the GetOrganelle assembly single k-mer (131-mer) and for *A. hemigymnus*

the metaSPAdes assembly with the maximum allowed k-mer size (127-mer). Every generated assembly was annotated with MitoZ (as described above). Read coverage distributions were analysed by aligning PE reads to the final genome assemblies using the Burrows-Wheeler Aligner (BWA) v.0.7.17-r1198 (Li 2013) and visualized in Artemis v17.0.1 (Carver et al. 2012) (fig. S7).

The Nanopore reads of *A. aculeatus* were quality-filtered using Filtlong (https://github.com/rrwick/Filtlong). Given that long repetitive regions seem to cause problems with the PE-based assemblies, the Nanopore reads were filtered by size (i.e., >21,000bp) to include only reads spanning the whole mitogenome. The mitogenome assembly was performed using Unicycler v.0.4.8. (Wick et al. 2017)). The assembly was polished, following the author's suggestions, with the Nanopore reads using medaka v1.2.2 (https://github.com/nanoporetech/medaka) and with short-reads, first using Polypolish v0.4.3 (Wick and Holt 2022) and after using Polca (Zimin and Salzberg 2020). Genome annotation was performed with MitoZ (as described above). Read coverage distributions were analysed by aligning PE reads (as described above).

Finally, since the *Sternoptyx obscura* mitogenome available on NCBI (OP057081) is marked as “UNVERIFIED” and therefore no annotation is provided, the mitogenome was downloaded and annotated using MitoZ (as described above).

To identify the putative Control Region (CR) of the deep sea hatchet fish mitogenome assemblies, we search for conserved motifs within non-coding regions to identify any of the known Conserved Sequence Blocks (CSB) that are involved in the replication initiation (Satoh et al. 2016). The recently described CSBs of several fish species were here used as a reference to guide the search, including one Stomifformes, i.e. *Diplophos taenia* (Satoh et al. 2016). We focused on the two most conserved of the

three CSBs, i.e., CSB-II and CSB-III. Given the lack of significant non-coding regions within the mitogenomes of *M.muelleri*, *A. affinis*, and *A. olfersii* (see Results and Discussion), these mitogenomes were not included in the analysis. Moreover, given the highly disproportionate read coverage distribution in the mitogenome non-coding regions of *A. hemigymnus* (fig. S7), this mitogenome was not considered. The coverage distribution indicates regions likely represented by the collapse of a highly repetitive region, thus not suited for the analysis. The non-coding regions from the remaining deep-sea hatchet fish species, the Antarctic Trematominae species, *Pagothenia borchgrevinkias* (with the only other record CDS mitochondrial inversion), as well as all the fish CSB-II and CSB-III identified by Satoh et al. (2016) were used. The sequences were uploaded to MEME v.5.5.2 (Bailey and Elkan 1994) and the Motif Discovery model was used to identify conserved motifs across all sequences, specifying a maximum motif width of 25.

Phylogenetic reconstruction

To produce a phylogenetic reconstruction, the whole mitogenomes of all Stomiiformes available on NCBI (n=15), including four Sternoptychidae species (i.e., *S. obscura, M. muelleri*, *P. polli*, *A. affinis*), the mitogenomes here produced and four outgroup taxa were used (Table 1). Alignments of the 13 protein-coding genes (PCGs) were produced using MAFFT v7.453 (Katoh and Standley 2013). Positions with gaps in 50% or more of the individual alignments were removed using trimAL v. 1.2rev59 (Capella-Gutiérrez et al. 2009) and all alignments were concatenated using FASconCAT-G (https://github.com/PatrickKueck/FASconCAT-G). The alignment composed by the concatenated PCGs from 15 species had a total length of 11,436 bp. The partition scheme and the evolutionary models that best fit those schemes, as

well as Maximum Likelihood (ML) phylogenetic inference were produced in IQ-TREE v.1.6.12 (Nguyen et al. 2015; Kalyaanamoorthy et al. 2017).

For the amino acid phylogenetic reconstruction, individual alignments were translated to proteins using the EMBOSS seqret V.6.6.0.0, trimmed with trimAL v. 1.2rev59 (as described above) and concatenated using FASconCAT-G. The alignment composed by the concatenated PCGs from 15 species had a total length of 3,801 aa. The partition scheme and the evolutionary models that best fit those schemes, as well as Maximum Likelihood (ML) phylogenetic inference were produced in IQ-TREE v.1.6.12.

COI Phylogeny

To produce a phylogenetic reconstruction with a wider taxa representation, all COI sequences available on GenBank (n=261) were downloaded (including the outgroup taxa *C. clupeaformis*). Alignment was performed using MAFFT v7.453 (Katoh and Standley 2013) and an ML phylogenetic inference was constructed in IQ-TREE v.1.6.12, also estimating the best evolutionary model for the analysis.

Strand-specific 4-fold redundant sites GC/AT skew estimations

The protein-coding genes of the complete mitogenomes of all vertebrates available in GenBank (http:// www.ncbi.nlm.nih.gov) in May of 2022 were retrieved. The calculation of the GC skew (G-C)/(G+C) and the AT skew (A-T)/(A+T) at 4-fold redundant sites using custom Perl scripts (Fonseca et al. 2014). The redundant codons examined were alanine (GCN), proline (CCN), serine (TCN), threonine (ACN), arginine (CGN), glycine (GGN), leucine (CTN), and valine (GTN).

Furthermore, to infer GC/AT skew inversions in other species from family Sternoptychidae, for which no whole mitogenome is available, the COI sequences for all Sternoptychidae species available on GenBank were downloaded and the calculations applied, as described above.

Whole Genome size estimation

The high coverage WGS PE sequencing reads for *A. aculeatus* and *S. diaphana* were used to estimate the overall characteristics of each species' genomes using Jellyfish v.2.2.10 and GenomeScope2 (Ranallo-Benavidez et al. 2020) with a k-mers length of 21.

Data Availability Statement

The raw sequencing reads and mtDNA assemblies are deposited at NCBI, and respective SRA and assembly accessions are depicted in Table 1, all linked to BioProject PRJNA977192.

Funding

AGS was funded by grant 2023_033_BI_ATLANTIDA, under the Project "ATLANTIDA - Platform for the monitoring of the North Atlantic Ocean and tools for the sustainable exploitation of the marine resources" (NORTE-01-0145-FEDER-000040), co-financed by Portugal 2020 and the European Union through Program FEDER. EF is funded by the Portuguese Foundation for Science and Technology (FCT) under grant CEECINST/00027/2021. This research was developed under the

493 project ATLANTIDA - Platform for the monitoring of the North Atlantic Ocean and
494 tools for the sustainable exploitation of the marine resources" (NORTE-01-0145-
495 FEDER-000040). Additional strategic funding was provided by FCT
496 UIDB/04423/2020 and UIDP/04423/2020. EU-Spain NAFO Groundfish survey has
497 been co-funded by the European Union through the European Maritime and
498 Fisheries Fund (EMFF) within the National Program of collection, management and
499 use of data in the fisheries sector and support for scientific advice regarding the
500 Common Fisheries Policy and IEO BIOPESLE project. The Spanish Bottom Trawl
501 Survey on the Porcupine Bank (SP-PORC-Q3) was funded in part by the EU through
502 the European Maritime and Fisheries Fund (EMFF) within the Spanish National
503 Program of Collection, Management and Use of Data in the Fisheries Sector and
504 Support for Scientific Advice Regarding the Common Fisheries Policy.

505

506

507 **FIGURE AND TABLE LEGENDS**

508

509 FIG.1. Left: Schematic representation of circular mitochondrial molecule highlighting
510 the protein-coding genes encoded in the different strands. Right: Representation of
511 linearized mitochondrial molecule, depicting the standard vertebrate gene order
512 shared by the deep-sea hatchetfish species, *Polyipnus polli*, *Maurolicus muelleri* and
513 *Argyropelecus affinis*. Genes encoded in the L-strand are depicted in red; Genes
514 encoded in the H-strand are depicted in white. * Control Region has not been
515 sequenced in either *Maurolicus muelleri* or *Argyropelecus affinis*. The CSB-II
516 sequence is a representation of the generally expected composition of the motif.

517

518 FIG.2. Left: Schematic representation of circular mitochondrial molecule highlighting
519 the protein-coding genes encoded in the different strands. Right: Representation of
520 linearized mitochondrial molecule, depicting the standard vertebrate gene order
521 (middle) comparatively to deep-sea hatchetfish species, *Sternoptyx obscura*,
522 *Sternoptyx diaphana*. Genes encoded in the L-strand are depicted in red; Genes
523 encoded in the H-strand are depicted in white; Red shadow represents
524 macrosyntenic patterns of gene inversion. The CSB-II sequence for the typical
525 vertebrate mtDNA is a representation of the generally expected composition of the
526 motif. The CSB-II sequences for the marine hatchet fish are the ones here identified.
527
528 FIG.3. Left: Schematic representation of circular mitochondrial molecule highlighting
529 the protein-coding genes encoded in the different strands. Right: Representation of
530 linearized mitochondrial molecule, depicting the standard vertebrate gene order
531 (second from the top) comparatively to deep-sea hatchetfish species, *Argyropelecus*
532 *hemingymnus*, *Argyropelecus aculeatus* and *Argyropelecus olfersii*. Genes encoded
533 in the L-strand are depicted in red; Genes encoded in the H-strand are depicted in
534 white; Red shadow represents macrosyntenic patterns of gene inversion; Grey
535 shadow represents macrosyntenic patterns of genes in the same strand. The CSB-II
536 sequence for the typical vertebrate mtDNA is a representation of the generally
537 expected composition of the motif. The CSB-II sequences for the marine hatchet fish
538 are the ones here identified.
539
540 FIG.4. a) IQ-tree Maximum Likelihood (ML) phylogenetic inference retrieved from the
541 nucleotide alignment of the 13 mitogenomes concatenated protein-coding genes. b)
542 IQ-tree Maximum Likelihood (ML) phylogenetic inference retrieved from the

543 nucleotide alignment of all available COI sequences of deep-sea hatchetfish in NCBI.
544 Above the nodes are represented ultrafast bootstrap values above 80%.
545
546 FIG.5. Top: Strand-specific 4-fold redundant sites GC/AT skew estimations for all
547 protein-coding genes, for four model vertebrate species with standard vertebrate
548 mitogenome gene order, each species of deep-sea hatchetfish analysed and one
549 representative species from the Antarctic fish subfamily Trematominae that have an
550 inversion of the ND1 and CR (inside the box). Bottom: Strand-specific 4-fold
551 redundant sites GC/AT skew estimations for COI mitochondrial gene of all deep-sea
552 hatchetfish, available in NCBI. Red shadows highlight the inversion of the strand-
553 specific nucleotide GC/AT skew pattern. Middle: Schematic representation of circular
554 mitochondrial molecule highlighting the protein-coding genes encoded in the different
555 strands.
556
557 FIG.6. Plots of the GC and AT skews at the 4-fold redundant sites of the
558 mitochondrial protein-coding genes ND1, ND2, COX1 and ND6 from 6,297 vertebrate
559 species. Dots represent each of the 6,297 analysed vertebrate species, with red
560 (deep-sea hatchetfish) and green (other fish species) dots highlighting genes with
561 inverted AT and GC skews. The plots for the remaining protein-coding genes are
562 provided in fig.S4.
563
564 Table 1. List of whole mitogenomes used in the whole mitogenome-based phylogeny.
565 * represent mitogenomes sequenced in this study.
566

FIG.S1. Schematic representation of the MEME - Motif discovery results, including the inferred conserved motif representing CSB-II (in red) and, in some species, CSB-III (in blue). The results include several CR from fish species studied in Satoh et al (2016) (using the same abbreviated nomenclature), as well as the non-coding regions of the deep-sea marine hatchet fish species *Sternoptyx obscura*, *Sternoptyx diaphana*, *Argyropelecus aculeatus*, the Stomiiformes species *Diplophos taenia,* and the Antarctic Trematominae species *Pagothenia borchgrevinki.*

FIG.S2. Complete circular mitochondrial molecule of the deep-sea hatchetfish species *Argyropelecus aculeatus*, produced by CGView/Proksee (https://proksee.ca).

FIG.S3. IQ-tree Maximum Likelihood (ML) phylogenetic inference retrieved from the amino acid alignments of the 13 concatenated mitogenome protein-coding genes. Above the nodes are represented ultrafast bootstrap values.

FIG.S4. Plots of the GC and AT skews at the 4-fold redundant sites of the mitochondrial protein-coding genes ND3, ND4, ND4L, ND5, COX2, COX3, CYTB, ATP6 ATP8 from 6,297 vertebrate species. Dots represent each of the 6,297 analysed vertebrate species, with red (deep-sea hatchetfish) and green (other fish species) dots highlighting genes with inverted AT and GC skews. The plots for the remaining protein-coding genes are provided in fig.6.

FIG.S5. Strand-specific 4-fold redundant sites GC/AT skew estimations for all protein-coding genes, for all mitogenomes of notothenioid fishes available on NCBI. Coloured circles represent the mitochondrial gene orders described by Papetti et al.

2021. Species not studied by Papetti et al. 2021 are in the black box. Mitogenomes with an inversion of the ND1 gene are highlighted in a thick red box.

FIG.S6. GenomeScope2 k-mer (21) distributions displaying estimation of genome size (len), homozygosity (aa), heterozygosity (ab), mean k-mer coverage for heterozygous bases (kcov), read error rate (err), the average rate of read duplications (dup), k-mer size used on the run (k:), and ploidy (p:) for *Argyropelecus aculeatus* (left) and *Sternoptyx diaphana* (right).

FIG.S7. Artemis read coverage plot distribution across the assembled marine hatchet fish mitogenome assemblies.

Supplementary File 1 - MEME - Motif discovery results, including the sequences of the inferred conserved motif representing CSB-II and, in some species, CSB-III. The results include all the CR of the fish species studied in Satoh et al (2016) (using the same abbreviated nomenclature), as well as the non-coding regions deep-sea marine hatchet fish species *Sternoptyx obscura*, *Sternoptyx diaphana*, *Argyropelecus aculeatus*, the Stomiiformes species *Diplophos taenia,* and the Antarctic Trematominae species *Pagothenia borchgrevinki*.

Supplementary File 2 - COI alignment including 261 sequences from 26 distinct deep-sea marine hatchetfish species and the outgroup species, i.e., *Coregonus clupeaformis* (Mitchill, 1818) (total length of 652 bp).

References

Arrondo NV, Gomes-dos-Santos A, Román Marcote E, Pérez M, Froufe E, Castro LFC. 2020. A new gene order in the mitochondrial genome of the deep-sea diaphanous hatchet fish Sternoptyx diaphana Hermann, 1781 (Stomiiformes: Sternoptychidae). *Mitochondrial DNA B Resour* [Internet] 5:2859–2861. Available from: https://www.tandfonline.com/doi/full/10.1080/23802359.2020.1790325

Bailey TL, Elkan C. 1994. Fitting a mixture model by expectation maximization to discover motifs in biopolymers. *Proceedings of the Second International Conference on Intelligent Systems for Molecular Biology* 2:28–36.

Bankevich A, Nurk S, Antipov D, Gurevich AA, Dvorkin M, Kulikov AS, Lesin VM, Nikolenko SI, Pham S, Prjibelski AD, et al. 2012. SPAdes: A New Genome Assembly Algorithm and Its Applications to Single-Cell Sequencing. *Journal of Computational Biology* [Internet] 19:455–477. Available from: http://www.liebertpub.com/doi/10.1089/cmb.2012.0021

Barshad G, Marom S, Cohen T, Mishmar D. 2018. Mitochondrial DNA Transcription and Its Regulation: An Evolutionary Perspective. *Trends in Genetics* 34:682–692.

Blumberg A, Rice EJ, Kundaje A, Danko CG, Mishmar D. 2017. Initiation of mtDNA transcription is followed by pausing, and diverges across human cell types and during evolution. *Genome Res* 27:362–373.

Blumberg A, Sailaja BS, Kundaje A, Levin L, Dadon S, Shmorak S, Shaulian E, Meshorer E, Mishmar D. 2014. Transcription Factors Bind Negatively Selected Sites within Human mtDNA Genes. *Genome Biol Evol* [Internet] 6:2634–2646. Available from: https://academic.oup.com/gbe/article/6/10/2634/610683

636 Bolger AM, Lohse M, Usadel B. 2014. Trimmomatic: a flexible trimmer for Illumina sequence data.
637 *Bioinformatics* [Internet] 30:2114–2120. Available from:
638 https://academic.oup.com/bioinformatics/article-lookup/doi/10.1093/bioinformatics/btu170

639 Boore JL. 1999. Animal mitochondrial genomes. *Nucleic Acids Res* [Internet] 27:1767–1780. Available
640 from: https://academic.oup.com/nar/article/27/8/1767/2847916

641 Calcino A, Baranyi C, 1 , Wanninger A. 2020. Heteroplasmy and repeat expansion in the plant-like
642 mitochondrial genome of a bivalve mollusc. *bioRxiv* [Internet]:2020.09.23.310516. Available
643 from: https://www.biorxiv.org/content/10.1101/2020.09.23.310516v2

644 Capella-Gutiérrez S, Silla-Martínez JM, Gabaldón T. 2009. trimAl: A tool for automated alignment
645 trimming in large-scale phylogenetic analyses. *Bioinformatics* [Internet] 25:1972–1973.
646 Available from: https://academic.oup.com/bioinformatics/article/25/15/1972/213148

647 Carnevale G. 2008. Miniature deep-sea hatchetfish (Teleostei: Stomiiformes) from the Miocene of
648 Italy. *Geol Mag* [Internet] 145:73–84. Available from:
649 https://www.cambridge.org/core/journals/geological-magazine/article/miniature-deepsea-
650 hatchetfish-teleostei-stomiiformes-from-the-miocene-of-
651 italy/F6121BE08716E80EA7731CC94A62DAB6

652 Carver T, Harris SR, Berriman M, Parkhill J, McQuillan JA. 2012. Artemis: an integrated platform for
653 visualization and analysis of high-throughput sequence-based experimental data. *Bioinformatics*
654 [Internet] 28:464–469. Available from:
655 https://academic.oup.com/bioinformatics/article/28/4/464/213043

656 Clayton DA. 1982. Replication of animal mitochondrial DNA. *Cell* 28:693–705.

657 Coad BW. 2019. Family Sternoptychidae – Marine Hatchetfishes, haches d'argent. *Marine Fishes of*
658 *Arctic Canada*:305–307.

659 Eduardo LN, Bertrand A, Mincarone MM, Santos L V., Frédou T, Assunção R V., Silva A, Ménard F,
660 Schwamborn R, Le Loc'h F, et al. 2020. Hatchetfishes (Stomiiformes: Sternoptychidae)
661 biodiversity, trophic ecology, vertical niche partitioning and functional roles in the western
662 Tropical Atlantic. *Prog Oceanogr* 187:102389.

663 Fonseca MM, Harris DJ, Posada D. 2014. The Inversion of the Control Region in Three Mitogenomes
664 Provides Further Evidence for an Asymmetric Model of Vertebrate mtDNA Replication. *PLoS*
665 *One* [Internet] 9:e106654. Available from:
666 https://journals.plos.org/plosone/article?id=10.1371/journal.pone.0106654

667 Fonseca MM, Posada D, Harris DJ. 2008. Inverted Replication of Vertebrate Mitochondria. *Mol Biol*
668 *Evol* [Internet] 25:805–808. Available from: https://academic.oup.com/mbe/article-
669 lookup/doi/10.1093/molbev/msn050

670 Formenti G, Rhie A, Balacco J, Haase B, Mountcastle J, Fedrigo O, Brown S, Capodiferro MR, Al-Ajli
671 FO, Ambrosini R, et al. 2021. Complete vertebrate mitogenomes reveal widespread repeats and
672 gene duplications. *Genome Biol* [Internet] 22:1–22. Available from:
673 https://genomebiology.biomedcentral.com/articles/10.1186/s13059-021-02336-9

674 Francino MP, Ochman H. 1997. Strand asymmetries in DNA evolution. *Trends in Genetics* 13:240–
675 245.

676 Ghiselli F, Gomes-dos-Santos A, Adema CM, Lopes-Lima M, Sharbrough J, Boore JL. 2021. Molluscan
677 mitochondrial genomes break the rules. *Philosophical Transactions of the Royal Society B:*
678 *Biological Sciences* [Internet] 376:20200159. Available from:
679 https://royalsocietypublishing.org/doi/10.1098/rstb.2020.0159

680 Gissi C, Pesole G, Mastrototaro F, Iannelli F, Guida V, Griggio F. 2010. Hypervariability of Ascidian
681 Mitochondrial Gene Order: Exposing the Myth of Deuterostome Organelle Genome Stability.

682 *Mol Biol Evol* [Internet] 27:211–215. Available from:
683 https://academic.oup.com/mbe/article/27/2/211/968133

684 Gjoesaeter J, Kawaguchi K. 1980. A review of the world resources of mesopelagic fish. *FAO Fisheries*
685 *Technical Papers (FAO)*.

686 Gong L, Shi W, Wang ZM, Miao XG, Kong XY. 2013. Control region translocation and a tRNA gene
687 inversion in the mitogenome of Paraplagusia japonica (Pleuronectiformes: Cynoglossidae).
688 *http://dx.doi.org/10.3109/19401736.2013.773984* [Internet] 24:671–673. Available from:
689 https://www.tandfonline.com/doi/abs/10.3109/19401736.2013.773984

690 Haddock SHD, Moline MA, Case JF. 2009. Bioluminescence in the Sea.
691 *https://doi.org/10.1146/annurev-marine-120308-081028* [Internet] 2:443–493. Available from:
692 https://www.annualreviews.org/doi/abs/10.1146/annurev-marine-120308-081028

693 Howell WH, Krueger WH. 1987. Family Sternoptychidae, marine hatchetfishes and related species.
694 Smithsonian contributions to zoology. In: GIBBS RH, KRUEGER WH, editors. Biology of Midwater
695 Fishes of the Bermuda Ocean Acre. Vol. 452. Washington, D.C.: Smithsonian Institution Press. p.
696 32–50.

697 Ijichi M, Takano T, Hasegawa M, Yashiki H, Kogure K, Kojima S, Yoshizawa S. 2018. The complete
698 mitochondrial genome of the longfin dragonfish Tactostoma macropus (Stomiiformes:
699 Stomiidae). *Mitochondrial DNA B Resour* [Internet] 3:486–487. Available from:
700 https://www.tandfonline.com/doi/full/10.1080/23802359.2018.1464411

701 Jin JJ, Yu W Bin, Yang JB, Song Y, Depamphilis CW, Yi TS, Li DZ. 2020. GetOrganelle: A fast and
702 versatile toolkit for accurate de novo assembly of organelle genomes. *Genome Biol* [Internet]
703 21:241. Available from: https://genomebiology.biomedcentral.com/articles/10.1186/s13059-
704 020-02154-5

705 Kalyaanamoorthy S, Minh BQ, Wong TKF, Von Haeseler A, Jermiin LS. 2017. ModelFinder: Fast model
706 selection for accurate phylogenetic estimates. *Nat Methods* [Internet] 14:587–589. Available
707 from: http://www.nature.com/articles/nmeth.4285

708 Katoh K, Standley DM. 2013. MAFFT multiple sequence alignment software version 7: Improvements
709 in performance and usability. *Mol Biol Evol* [Internet] 30:772–780. Available from:
710 https://academic.oup.com/mbe/article-lookup/doi/10.1093/molbev/mst010

711 Kennedy SR, Salk JJ, Schmitt MW, Loeb LA. 2013. Ultra-Sensitive Sequencing Reveals an Age-Related
712 Increase in Somatic Mitochondrial Mutations That Are Inconsistent with Oxidative Damage.
713 *PLoS Genet* 9:e1003794.

714 Kolesnikov AA, Gerasimov ES. 2012. Diversity of mitochondrial genome organization. *Biochemistry*
715 *(Moscow)* [Internet] 77:1424–1435. Available from:
716 https://link.springer.com/article/10.1134/S0006297912130020

717 Kong X, Dong X, Zhang Y, Shi W, Wang Z, Yu Z. 2009. A novel rearrangement in the mitochondrial
718 genome of tongue sole, Cynoglossus semilaevis: Control region translocation and a tRNA gene
719 inversion. *Genome* [Internet] 52:975–984. Available from:
720 https://cdnsciencepub.com/doi/abs/10.1139/G09-069

721 Krönström J, Holmgren S, Baguet F, Salpietro L, Mallefet J. 2005. Nitric oxide in control of
722 luminescence from hatchetfish(Argyropelecus hemigymnus) photophores. *Journal of*
723 *Experimental Biology* [Internet] 208:2951–2961. Available from:
724 https://journals.biologists.com/jeb/article/208/15/2951/15770/Nitric-oxide-in-control-of-
725 luminescence-from

726 Lee WJ, Conroy J, Howell WH, Kocher TD. 1995. Structure and evolution of teleost mitochondrial
727 control regions. *J Mol Evol* [Internet] 41:54–66. Available from:
728 https://link.springer.com/article/10.1007/BF00174041

729 Li H. 2013. Aligning sequence reads, clone sequences and assembly contigs with BWA-MEM.
730 Available from: http://arxiv.org/abs/1303.3997

731 Meng G, Li Y, Yang C, Liu S. 2019. MitoZ: a toolkit for animal mitochondrial genome assembly,
732 annotation and visualization. *Nucleic Acids Res* [Internet] 47:e63–e63. Available from:
733 https://doi.org/10.1093/nar/gkz173

734 Minhas BF, Beck EA, Cheng C-HC, Catchen J. 2023. Novel mitochondrial genome rearrangements
735 including duplications and extensive heteroplasmy could underlie temperature adaptations in
736 Antarctic notothenioid fishes. *Sci Rep* 13:6939.

737 Montaña-Lozano P, Moreno-Carmona M, Ochoa-Capera M, Medina NS, Boore JL, Prada CF. 2022.
738 Comparative genomic analysis of vertebrate mitochondrial reveals a differential of
739 rearrangements rate between taxonomic class. *Scientific Reports 2022 12:1* [Internet] 12:1–13.
740 Available from: https://www.nature.com/articles/s41598-022-09512-2

741 Nelson JS. 2016. Fishes of the World. 5th ed. (JohnWiley and Sons, editor.). New York, NY

742 Nguyen LT, Schmidt HA, Von Haeseler A, Minh BQ. 2015. IQ-TREE: A fast and effective stochastic
743 algorithm for estimating maximum-likelihood phylogenies. *Mol Biol Evol* [Internet] 32:268–274.
744 Available from: https://academic.oup.com/mbe/article-lookup/doi/10.1093/molbev/msu300

745 Nurk S, Meleshko D, Korobeynikov A, Pevzner PA. 2017. metaSPAdes: a new versatile metagenomic
746 assembler. *Genome Res* [Internet] 27:824–834. Available from:
747 https://genome.cshlp.org/content/27/5/824.full

748 Papetti C, Babbucci M, Dettai A, Basso A, Lucassen M, Harms L, Bonillo C, Heindler FM, Patarnello T,
749 Negrisolo E. 2021. Not Frozen in the Ice: Large and Dynamic Rearrangements in the
750 Mitochondrial Genomes of the Antarctic Fish. *Genome Biol Evol* [Internet] 13. Available from:
751 https://academic.oup.com/gbe/article/13/3/evab017/6133229

752 Parey E, Louis A, Montfort J, Guiguen Y, Crollius HR, Berthelot C. 2022. An atlas of fish genome
753 evolution reveals delayed rediploidization following the teleost whole-genome duplication.
754 *Genome Res* [Internet] 32:1685–1697. Available from:
755 https://genome.cshlp.org/content/32/9/1685.full

756 Ranallo-Benavidez TR, Jaron KS, Schatz MC. 2020. GenomeScope 2.0 and Smudgeplot for reference-
757 free profiling of polyploid genomes. *Nat Commun* [Internet] 11:1–10. Available from:
758 https://doi.org/10.1038/s41467-020-14998-3

759 Saccone C, Gissi C, Reyes A, Larizza A, Sbisà E, Pesole G. 2002. Mitochondrial DNA in metazoa: degree
760 of freedom in a frozen event. *Gene* 286:3–12.

761 Satoh TP, Miya M, Mabuchi K, Nishida M. 2016. Structure and variation of the mitochondrial genome
762 of fishes. *BMC Genomics* [Internet] 17:719. Available from:
763 http://bmcgenomics.biomedcentral.com/articles/10.1186/s12864-016-3054-y

764 Sharbrough J, Bankers L, Cook E, Fields PD, Jalinsky J, Mcelroy KE, Neiman M, Logsdonjr JM, Boore JL.
765 2023. Single-molecule Sequencing of an Animal Mitochondrial Genome Reveals Chloroplast-like
766 Architecture and Repeat-mediated Recombination. *Mol Biol Evol* [Internet] 40. Available from:
767 https://academic.oup.com/mbe/article/40/1/msad007/6980790

768 Shtolz N, Mishmar D. 2023. The metazoan landscape of mitochondrial DNA gene order and content is
769 shaped by selection and affects mitochondrial transcription. *Communications Biology 2023 6:1*
770 [Internet] 6:1–15. Available from: https://www.nature.com/articles/s42003-023-04471-4

771 Wick RR, Holt KE. 2022. Polypolish: Short-read polishing of long-read bacterial genome assemblies.
772 *PLoS Comput Biol* [Internet] 18:e1009802. Available from:
773 https://journals.plos.org/ploscompbiol/article?id=10.1371/journal.pcbi.1009802

774 Wick RR, Judd LM, Gorrie CL, Holt KE. 2017. Unicycler: Resolving bacterial genome assemblies from
775 short and long sequencing reads.Phillippy AM, editor. *PLoS Comput Biol* [Internet] 13:e1005595.
776 Available from: https://dx.plos.org/10.1371/journal.pcbi.1005595

777 Wick RR, Schultz MB, Zobel J, Holt KE. 2015. Bandage: interactive visualization of de novo genome
778 assemblies. *Bioinformatics* [Internet] 31:3350–3352. Available from:
779 https://doi.org/10.1093/bioinformatics/btv383

780 Zhang J, Kan X, Miao G, Hu S, Sun Q, Tian W. 2020. qMGR: A new approach for quantifying
781 mitochondrial genome rearrangement. *Mitochondrion* 52:20–23.

782 Zimin A V., Salzberg SL. 2020. The genome polishing tool POLCA makes fast and accurate corrections
783 in genome assemblies. *PLoS Comput Biol* [Internet] 16:e1007981. Available from:
784 https://journals.plos.org/ploscompbiol/article?id=10.1371/journal.pcbi.1007981

785

786

787

788

789

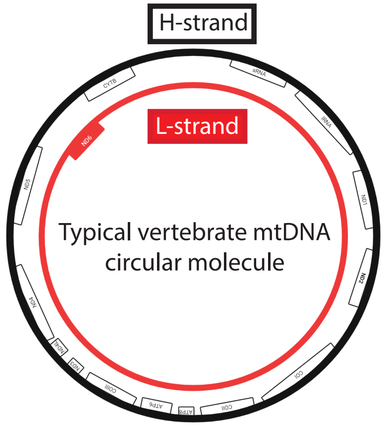

~16,000 kb

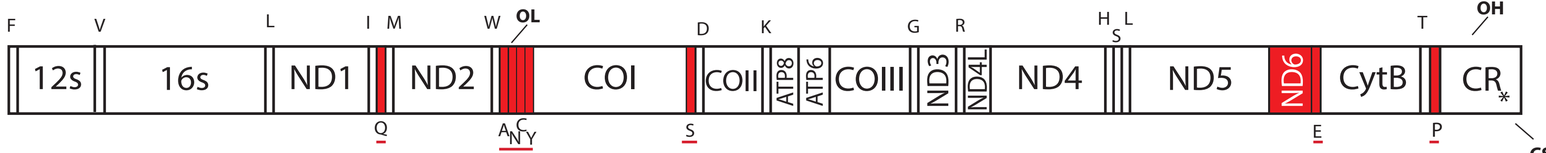

Typical vertebrate mtDNA

Polyipnus polli

~16,773 kb

Maurolicus muelleri

~15,230 kb

Argyropelecus affinis

~15,489 kb

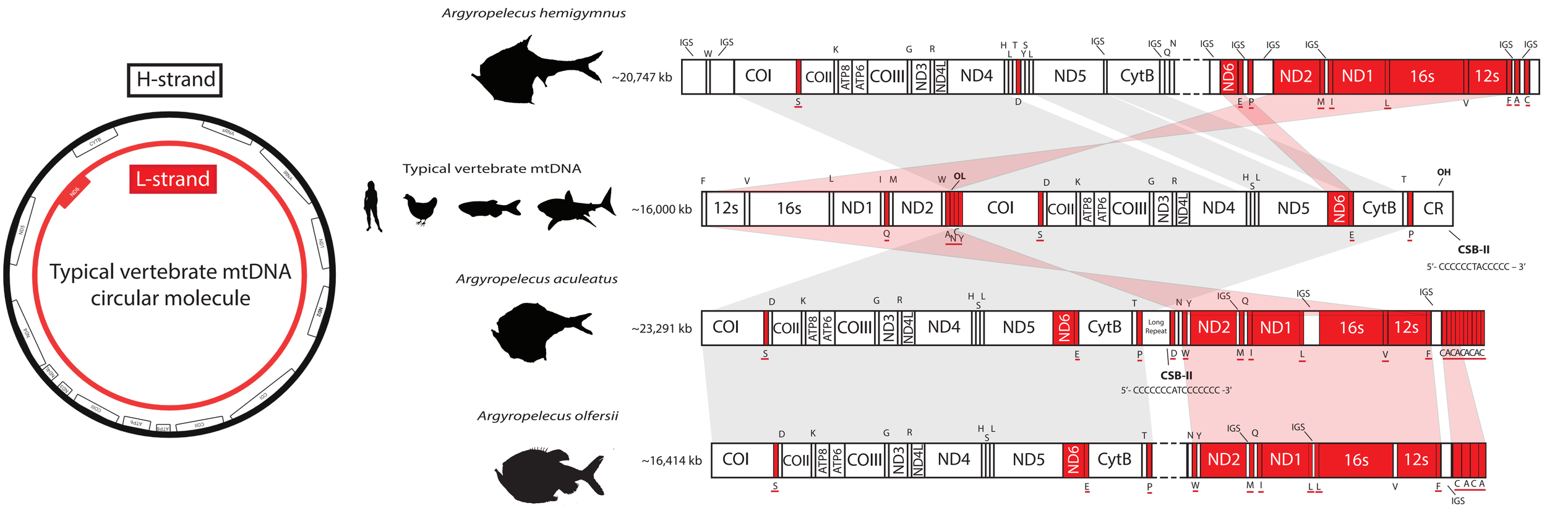
H-strand
L-strand
ND6
Typical vertebrate mtDNA
circular molecule
CYTB
tRNA
rRNA
16S
ND1
ND2
COI
ATP6
COII
tRNK
tRNS
tRNN
ND5
ND4
Argyropelecus hemigymnus
~20,747 kb
IGS W IGS K G R H T S L Y L IGS IGS N Q IGS IGS IGS IGS IGS IGS
COI COII ATP8 ATP6 COIII ND3 ND4L ND4 ND5 CytB ND6 ND2 ND1 16s 12s
S D E P M I L V F A C
Typical vertebrate mtDNA
~16,000 kb
F V L I M W OL D K G R H L S T OH
12s 16s ND1 ND2 COI COII ATP8 ATP6 COIII ND3 ND4L ND4 ND5 ND6 CytB CR
Q A C N Y S E P
CSB-II
5′- CCCCCCTACCCCC – 3′
Argyropelecus aculeatus
~23,291 kb
D K G R H L S T N Y IGS Q IGS IGS
COI COII ATP8 ATP6 COIII ND3 ND4L ND4 ND5 ND6 CytB Long Repeat ND2 ND1 16s 12s
S E P D W M I L V F CACACACAC
CSB-II
5′- CCCCCCCATCCCCCCC -3′
Argyropelecus olfersii
~16,414 kb
D K G R H L S T N Y IGS Q IGS
COI COII ATP8 ATP6 COIII ND3 ND4L ND4 ND5 ND6 CytB ND2 ND1 16s 12s
S E P W M I L L V F C A C A IGS

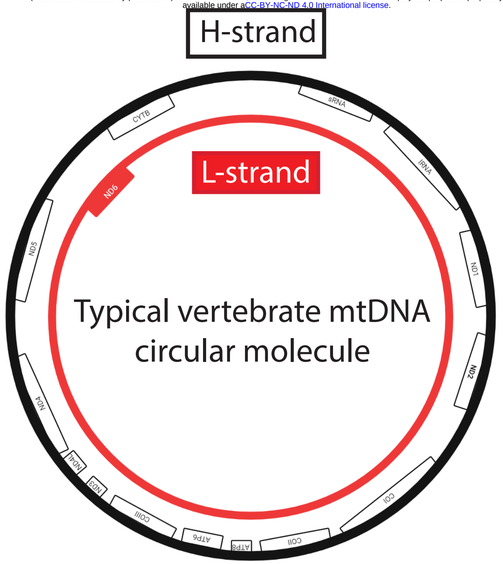

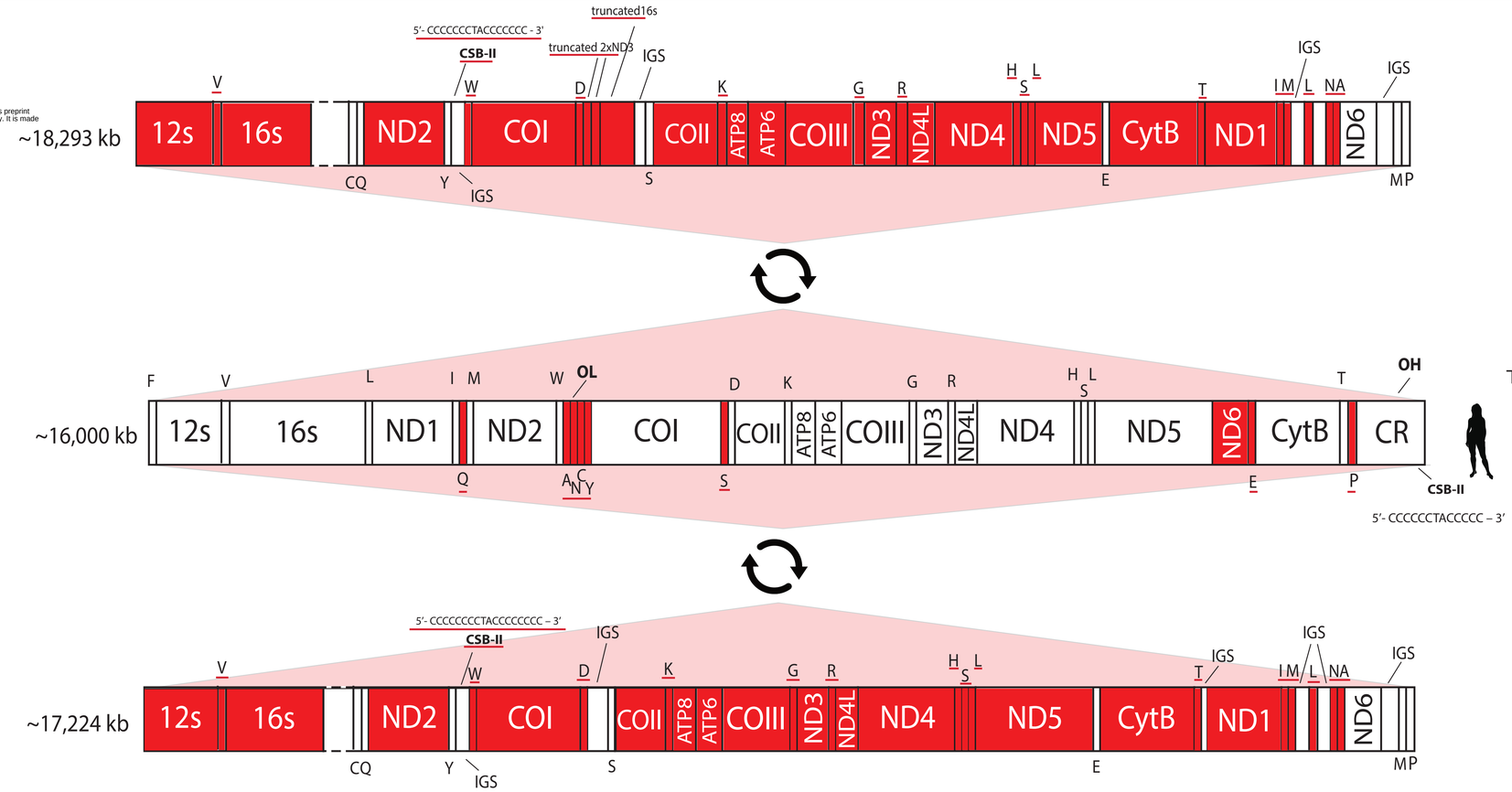

Sternoptyx obscura

Typical vertebrate mtDNA

Sternoptyx diaphana

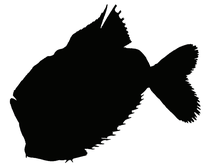

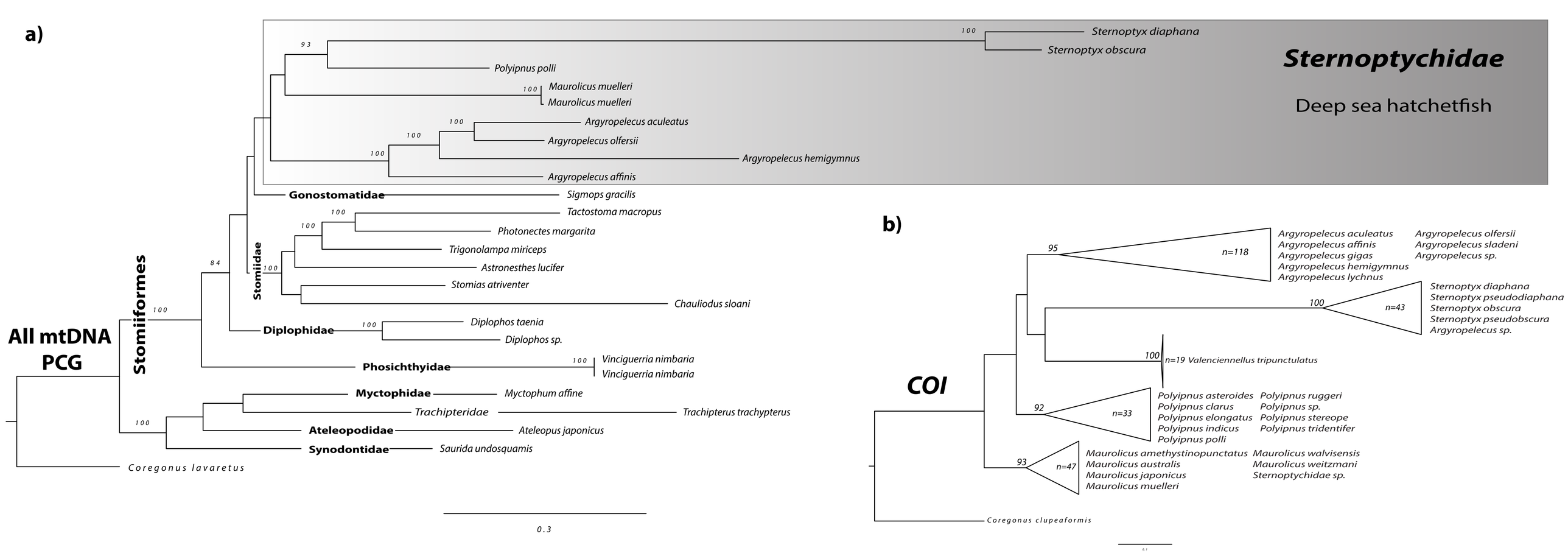
a)
Sternoptychidae
Deep sea hatchetfish
Sternoptyx diaphana
Sternoptyx obscura
Polyipnus polli
Maurolicus muelleri
Maurolicus muelleri
Argyropelecus aculeatus
Argyropelecus olfersii
Argyropelecus hemigymnus
Argyropelecus affinis
Gonostomatidae
Sigmops gracilis
Tactostoma macropus
Photonectes margarita
Trigonolampa miriceps
Astronesthes lucifer
Stomias atriventer
Chauliodus sloani
Stomiidae
Stomiiformes
Diplophidae
Diplophos taenia
Diplophos sp.
Phosichthyidae
Vinciguerria nimbaria
Vinciguerria nimbaria
Myctophidae
Myctophum affine
Trachipteridae
Trachipterus trachypterus
Ateleopodidae
Ateleopus japonicus
Synodontidae
Saurida undosquamis
Coregonus lavaretus
All mtDNA PCG
0.3
b)
COI
n=118
Argyropelecus aculeatus
Argyropelecus affinis
Argyropelecus gigas
Argyropelecus hemigymnus
Argyropelecus lychnus
Argyropelecus olfersii
Argyropelecus sladeni
Argyropelecus sp.
n=43
Sternoptyx diaphana
Sternoptyx pseudodiaphana
Sternoptyx obscura
Sternoptyx pseudobscura
Argyropelecus sp.
n=19 Valenciennellus tripunctulatus
n=33
Polyipnus asteroides
Polyipnus clarus
Polyipnus elongatus
Polyipnus indicus
Polyipnus polli
Polyipnus ruggeri
Polyipnus sp.
Polyipnus stereope
Polyipnus tridentifer
n=47
Maurolicus amethystinopunctatus
Maurolicus australis
Maurolicus japonicus
Maurolicus muelleri
Maurolicus walvisensis
Maurolicus weitzmani
Sternoptychidae sp.
Coregonus clupeaformis

GC skew

AT skew

Typical vertebrate structure

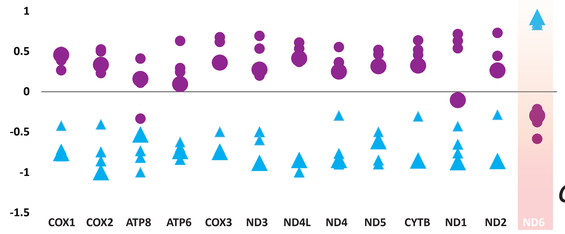

Homo sapiens

Gallus gallus

Danio rerio

Carcharodon carcharias

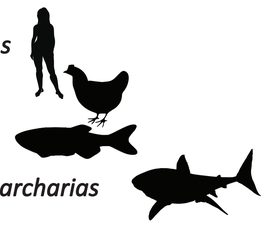

Argyropelecus aculeatus

Argyropelecus aculeatus

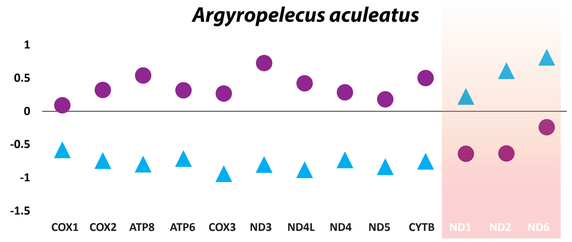

Argyropelecus olfersii

Argyropelecus olfersii

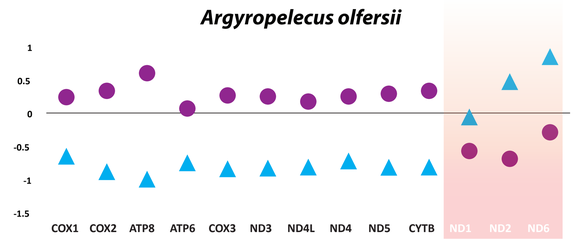

Argyropelecus hemigymnus

Argyropelecus hemigymnus

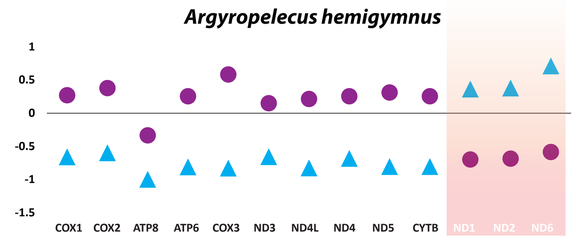

Sternoptyx diaphana
(MT588184.1)

Sternoptyx diaphana

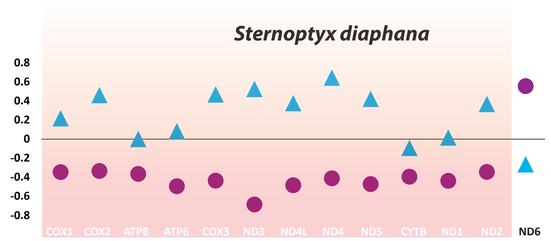

H-strand

L-strand

Typical vertebrate mtDNA
circular molecule

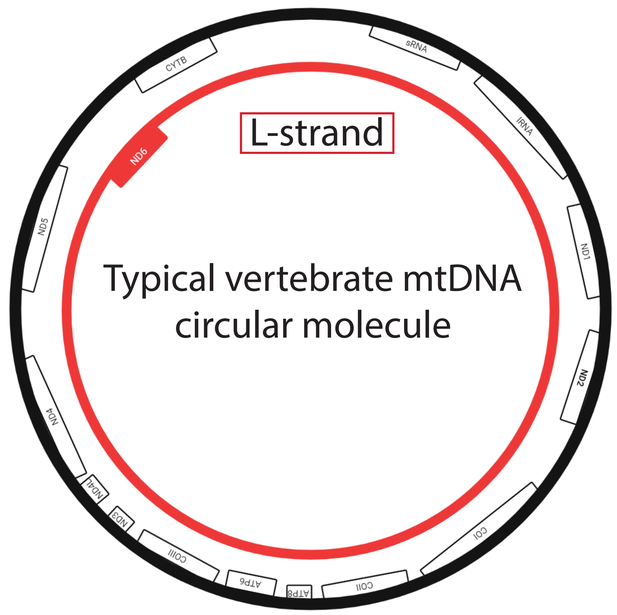

Trematomus eulepidotus
(MT559895.1)

Trematomus eulepidotus

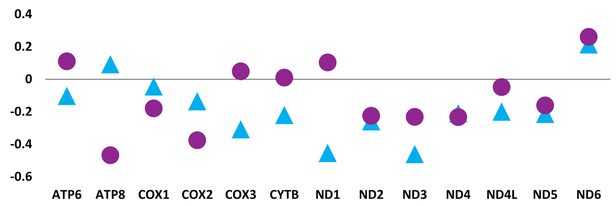

Antarctic notothenioid fish
(Trematominae)

Maurolicus muelleri

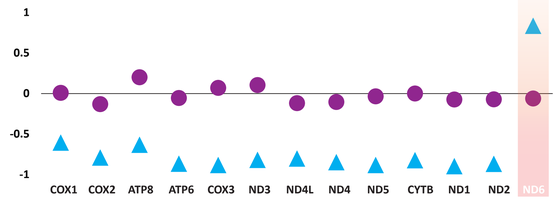

Maurolicus muelleri

Polyipnus polli

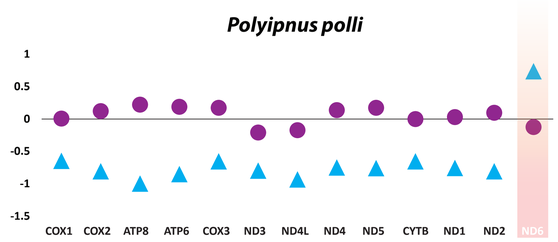

Polyipnus polli (AP012962)

Argyropelecus affinis

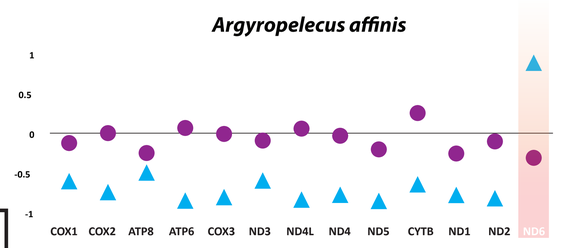

Argyropelecus affinis (AP012964.1)

Sternoptyx obscura

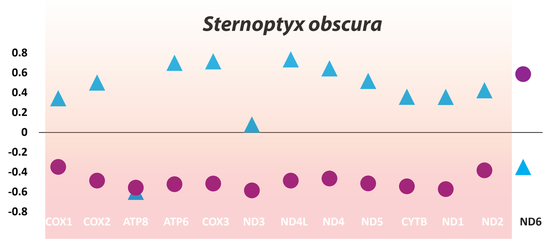

Sternoptyx obscura
(OP057081.1)

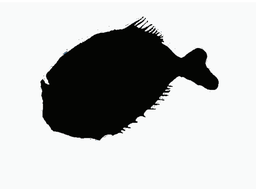

Sternoptychinae Cytochrome C Oxidase Subunit I (COX1)

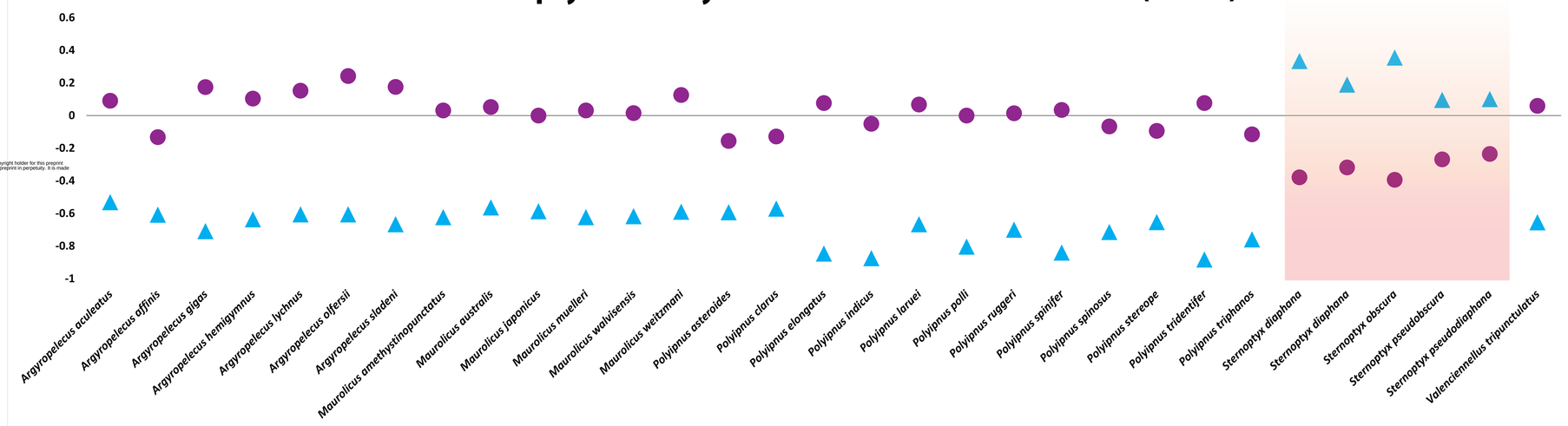

GC skew

AT skew

Argyropelecus	*Maurolicus*	*Polyipnus*	*Sternoptyx*	*Valenciennellus*

A)

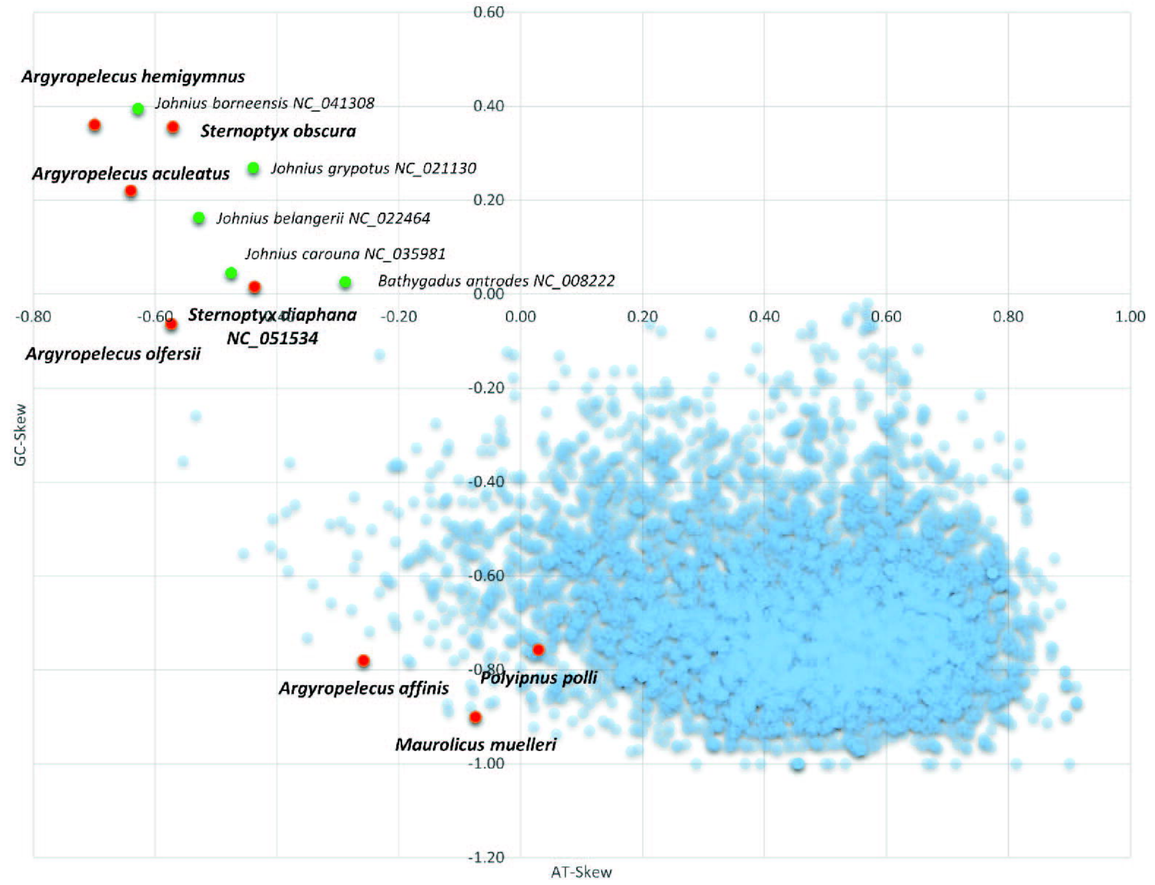

B)

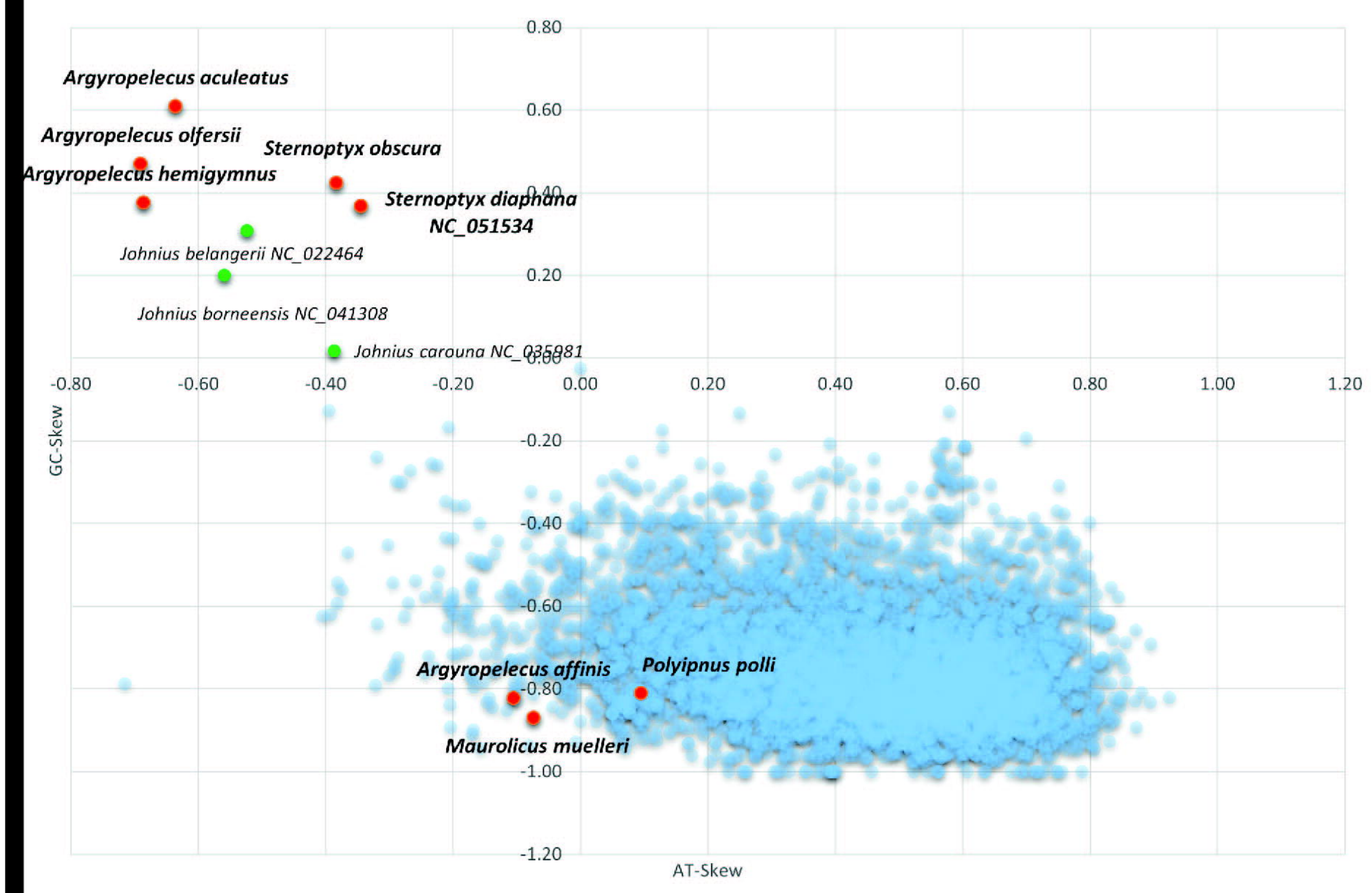

C)

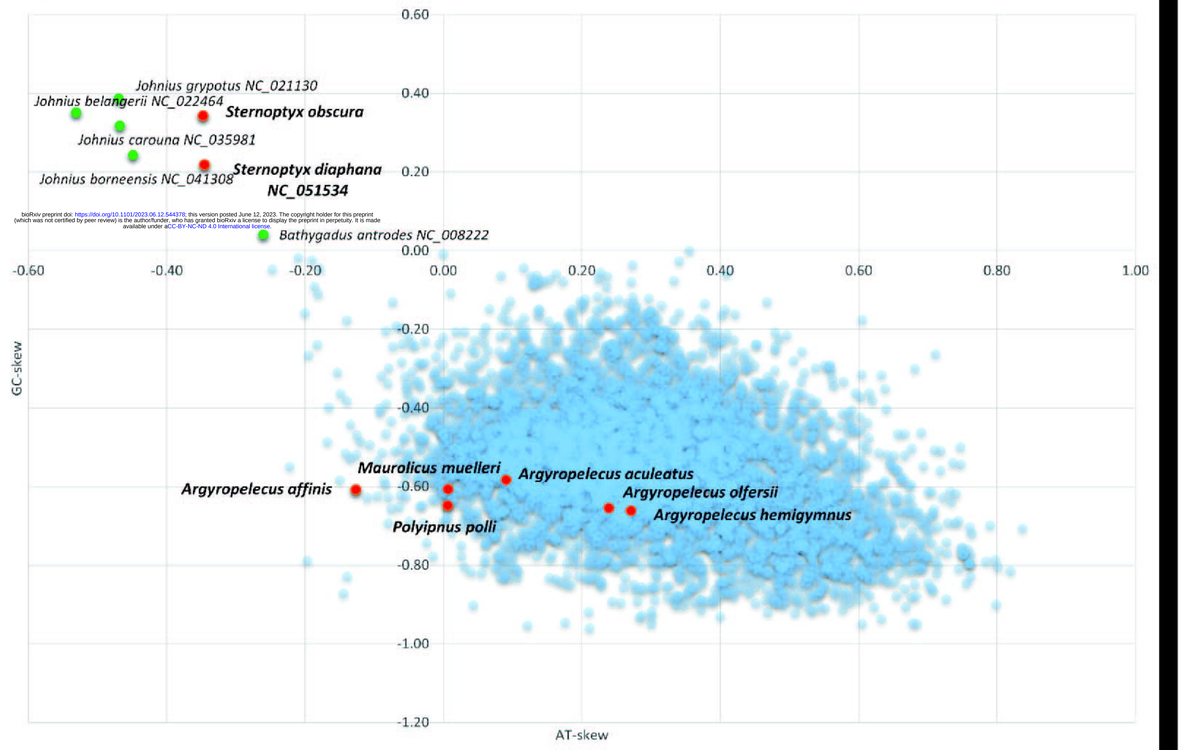

D)

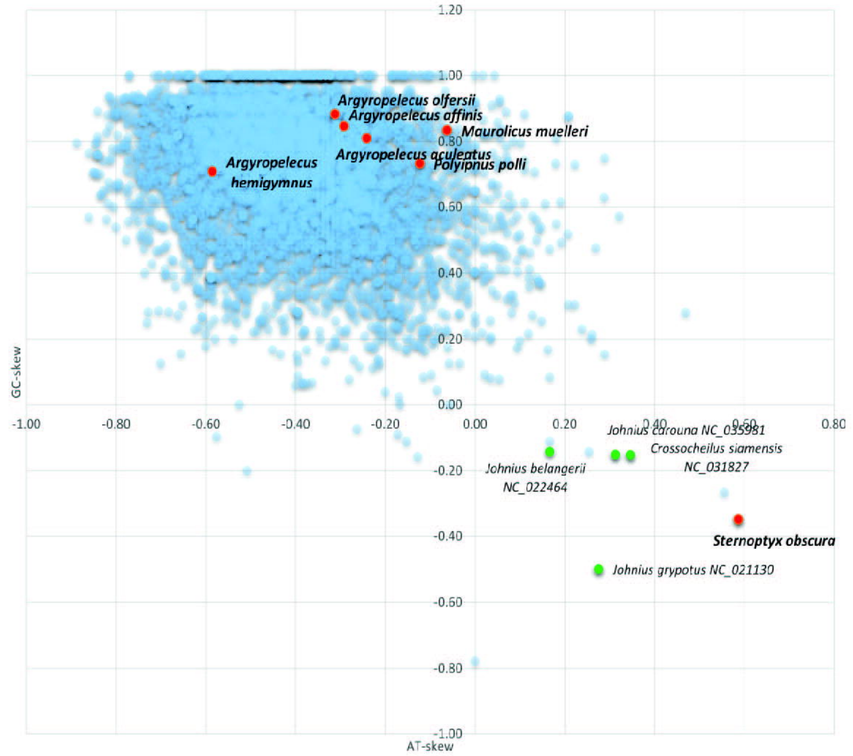

		GenBank Accession			
Sternoptychidae	*Argyropelecus aculeatus* *	OR062951	SAMN35453525	SRR24764805 and SRR24764804	15,291
Sternoptychidae	*Argyropelecus affinis*	AP012964.1	-	-	15,489
Sternoptychidae	*Argyropelecus hemigymnus* *	OR062952	SAMN35453526	SRR24764802	20,747
Sternoptychidae	*Argyropelecus olfersii* *	OR062953 and OR062954	SAMN35453527	SRR24764803	16,414
Sternoptychidae	*Maurolicus muelleri*	AP012963.1	-	-	15230
Sternoptychidae	*Maurolicus muelleri* *	OR062955	SAMN35453528	SAMN35453528	16,604
Sternoptychidae	*Polyipnus polli*	AP012962.1	-	SRR24764801	16773
Sternoptychidae	*Sternoptyx diaphana*	MT588184.1	SAMN35453678	SRR24764797-SRR24764800	17,224
Sternoptychidae	*Sternoptyx obscura*	OP057081.1	-	-	18,293
Gonostomatidae	*Sigmops gracilis*	AB016274.1	-	-	16,436
Stomiidae	*Tactostoma macropus*	LC377784.2	-	-	17,563
Stomiidae	*Photonectes margarita*	AP018417.1	-	-	18,592
Stomiidae	*Trigonolampa miriceps*	AP012961.1	-	-	15,709
Stomiidae	*Astronesthes lucifer*	AP012959.1	-	-	15,491
Stomiidae	*Stomias atriventer*	MG321595.1	-	-	17,596
Stomiidae	*Chauliodus sloani*	AP002915.1	-	-	17,814
Diplophidae	*Diplophos taenia*	AP012960.1	-	-	16,427
Diplophidae	*Diplophos sp.*	AB034825.1	-	-	16,418
Phosichthyidae	*Vinciguerria nimbaria*	AP006769.1	-	-	16,741
Phosichthyidae	*Vinciguerria nimbaria*	AP012958.1	-	-	16,741
Myctophum affine	*Myctophum affine*	AP002922.1	-	-	16,239
Trachipteridae	*Trachipterus trachipterus*	AP002925.1	-	-	16,162
Ateleopodidae	*Ateleopus japonicus*	AP002916.1	-	-	16,650
Synodontidae	*Saurida undosquamis*	AP002920.1	-	-	15,737
Salmonidae	*Coregonus lavaretus*	AB034824.1	-	-	16,737